Templated Formation of Luminescent Virus-like Particles by Tailor-Made Pt(II) Amphiphiles

Stephan Sinn,[†,‡,⊥] Liulin Yang,[∥,⊥] Frank Biedermann,[‡] Di Wang,[‡,§] Christian Kübel,[‡,§] Jeroen J. L. M. Cornelissen,*[∥] and Luisa De Cola*[†,‡]

[†]Institut de Science et d'Ingénierie Supramoléculaires (ISIS), Université de Strasbourg & CNRS, 8 Rue Gaspard Monge, 67000 Strasbourg, France

[‡]Institute of Nanotechnology (INT) and [§]Karlsruhe Nano Micro Facility, Karlsruhe Institute of Technology (KIT), Hermann-von-Helmholtz-Platz 1, 76344 Eggenstein-Leopoldshafen, Germany

[∥]Laboratory for Biomolecular Nanotechnology, MESA+ Institute, University of Twente, P.O. Box 207, 7500 AE Enschede, The Netherlands

S *Supporting Information*

ABSTRACT: Virus-like particles (VLPs) have been created from luminescent Pt(II) complex amphiphiles, able to form supramolecular structures in water solutions, that can be encapsulated or act as templates of cowpea chlorotic mottle virus capsid proteins. By virtue of a bottom-up molecular design, icosahedral and nonicosahedral (rod-like) VLPs have been constructed through diverse pathways, and a relationship between the molecular structure of the complexes and the shape and size of the VLPs has been observed. A deep insight into the mechanism for the templated formation of the differently shaped VLPs was achieved, by electron microscopy measurements (TEM and STEM) and bulk analysis (FPLC, DLS, photophysical investigations). Interestingly, the obtained VLPs can be visualized by their intense emission at room temperature, generated by the self-assembly of the Pt(II) complexes. The encapsulation of the luminescent species is further verified by their higher emission quantum yields inside the VLPs, which is due to the confinement effect of the protein cage. These hybrid materials demonstrate the potential of tailor-made supramolecular systems able to control the assembly of biological building blocks.

spherical VLPs / tubular VLPs
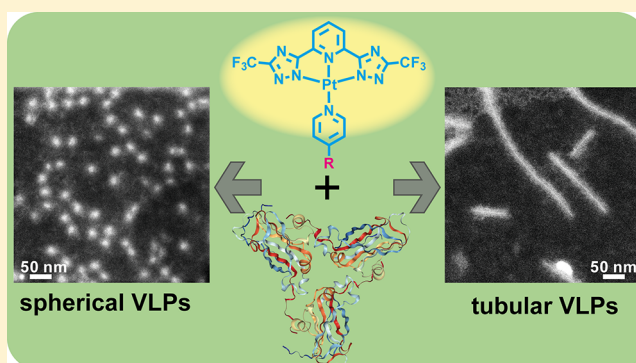
INTRODUCTION

Self-assembly is a powerful tool for the formation of large molecular architectures, able to perform complex functions.[1−6] An elegant paradigm for the duality of supramolecular morphology and function is represented by the natural virus capsid formation.[7−20] Natural viral capsid proteins (CPs) have a high preference for forming closed capsids, even in the absence of the naturally templating DNA or RNA.[21,22] As a representative, cowpea chlorotic mottle virus (CCMV) has been extensively explored as a nanocontainer and nanoreactor, with a wide spectrum of cargos including small molecules,[23] enzymes,[24] polymers,[25,26] micelles,[27,28] and nanoparticles.[29−34] For electric neutral cargos, a passive encapsulation can be adopted, resulting in distributions of both filled and empty icosahedral virus-like particles (VLPs) with a triangulation number of $T = 3$ (28 nm in diameter) structure.[27] For negatively charged cargos, a templated encapsulation is preferred, resulting in icosahedral VLPs filled by cargos with diverse structures ($T = 1, 2, 3$).[23] It should be noted that it is not necessary for the CCMV-based VLPs to be icosahedrons. Rigid covalent polymer- or DNA-based scaffolds are capable of

triggering the assembly of CPs around the scaffolds, resulting in nonicosahedral VLPs (e.g., rod-like particles).[18,35,36]

In spite of numerous studies of virus-based supramolecular nanostructures, a deep and systematic understanding of pathway complexity of self-assembly, as well as the resulting morphology and functionality, is elusive.[37,38] Modulation of cooperative and competitive driving forces including template–template interactions, template–protein interactions, and protein–protein interactions is essential to access a better control of self-assembly processes and target functions of VLPs.[38,39] The template effect is one of the most powerful tools for steering the resulting assembly size and shape.[40−43] For instance, templates that employ the comparably strong hydrogen-bonding interaction as a directional organization motif are widely utilized in supramolecular chemistry.[44,45]

Taking advantage of a bottom-up molecular design and assembly, it is feasible to establish an ideal integrative system to
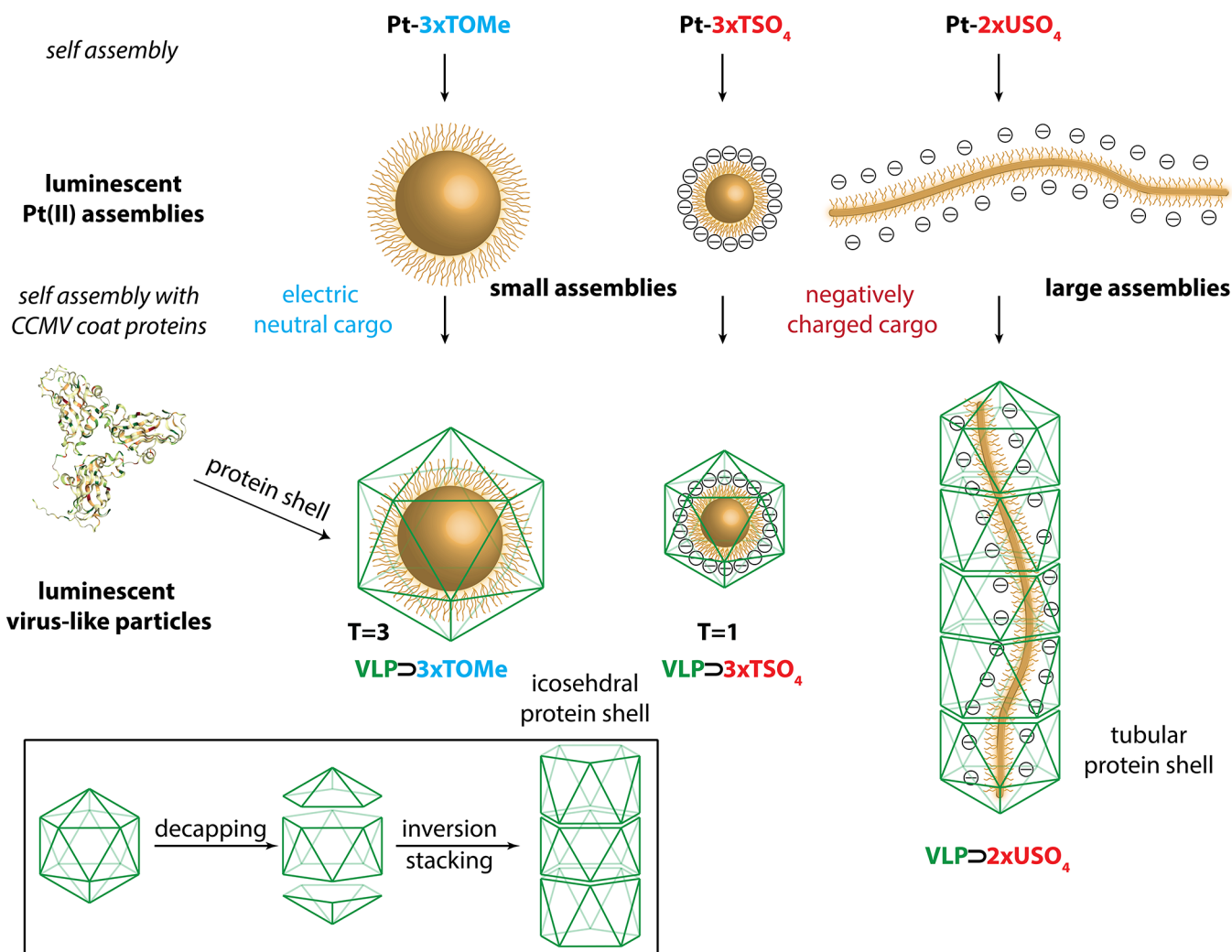
Figure 1. Formation of differently shaped virus-like particles depending on the chosen Pt(II) monomer. The proposed mechanism includes a preceding self-assembly of the Pt(II) amphiphiles featuring a subsequent self-assembly process with the CCMV coat proteins to spherical (icosahedral) or tubular luminescent virus-like particles. Inset: Schematic formation of tubular structures composed of subunits of "uncapped" icosahedrons.

gain insights into these complex relationships among structure, morphology, and function.

As the size and shape of self-assembled systems often determine the function (e.g., for proteins and DNA), it is of great importance to develop strategies for the control of the molecular assembly process.[46] In aqueous media, H-bonding and other directional noncovalent bonding motifs (e.g., dipole interactions) are efficiently screened by water as a solvent,[47] which complicates the design of suitable artificial templates. Moreover, hydrophobic and dispersion interactions are non-directional and energetically rather weak for small- and medium-sized organic molecules.[47−51] For instance, the aqueous self-assembly of common synthetic surfactants such as cetyltrimethylammonium bromide (CTAB) or sodium dodecyl sulfate (SDS) into micelles only occurs at greater than millimolar critical aggregation concentration (CAC).[52,53] In contrast, many biologically relevant systems form much more stable self-assembled structures in water, CAC ∼ nanomolar to micromolar for typical biological phospholipids.[54,55]

Recently, we have reported Pt(II) complexes capable of self-assembling into different emissive nanostructures.[56,57] Self-aggregation of Pt(II) complexes is promoted in solution by their square-planar geometry as well as $\pi-\pi$ and hydrophobic interactions of the ligands and at short distances (<3.5 Å) by Pt−Pt interactions.[58,59] Thus, it is expected that combining a hydrophobic Pt(II) complex moiety with hydrophilic tails will lead to amphiphiles that form thermodynamically stable self-assembled structures in water.

Here, we demonstrate how assembled amphiphilic platinum complexes can be encapsulated into VLPs or even act as templates to tailor the morphology of VLPs. To achieve our aim, we have synthesized a family of water-soluble platinum complexes which possess a strong emission once they are assembled in solution. The complexes contain a hydrophobic terdentate ligand and a pyridine unit, substituted with tetraethylene glycol or aliphatic chains, as ancillary ligand to complete the coordination sphere of the Pt(II) ion. We describe how, through subtle modulation of the charge, number, and nature (hydrophobic or hydrophilic) of the tails, we can obtain different morphologies of VLPs. In addition, the luminescence of the assemblies is influenced by the formation and by the morphology of the VLPs. The enhanced photophysical properties of the entrapped Pt(II) complexes,

that is, the aggregation-state-dependent emission and the role played by the confinement provided by the assembly of the proteins around the Pt complexes' supramolecular structures, allow for facile monitoring of the hybrid virus-like particle formation.

■ RESULTS AND DISCUSSION

Design, Synthesis, and Characterization of Pt(II) Complex Amphiphiles. The Pt(II) amphiphiles were based on a square-planar Pt(II) framework comprising a hydrophobic "head", a terdentate ligand (2,6-bis(3-(trifluoromethyl)-1H-1,2,4-triazol-5-yl)pyridine), and an ancillary pyridine substituted at position 4 with a hydrophilic moiety based on tetraethylene glycol chains or an alkyl chain. The chain can be neutral or negatively charged when terminated with sulfate units (Scheme 1). These compounds display advantageous

Scheme 1. Pt(II) Complexes Utilized for Encapsulation Experiments Featuring Double or Triple Branched Tetraethylene Glycol (T) or Undecyl (U) Side Chains That Are Terminated by Noncharged Methoxy (−OMe) or Hydroxy (−OH) or by Negatively Charged Sulfate (−SO₄⁻) Groups[a]
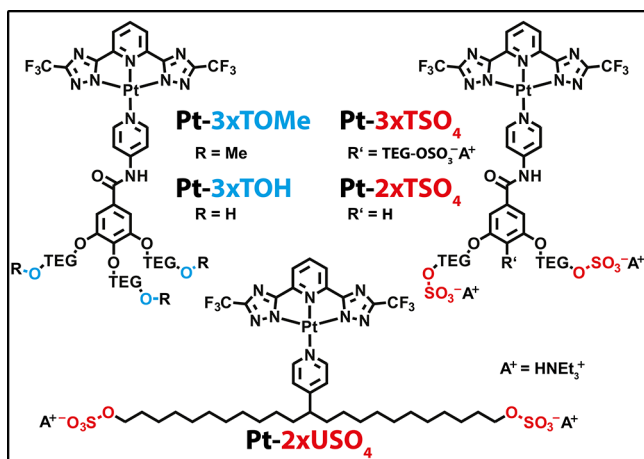
[a]See synthesis section in the SI for synthetic details and other compounds.

photophysical properties over its bis(tetrazole)−Pt(II)−pyridine analogue.[60−62] The hydrophilic "tails" were installed on the ancillary ligands through a simple etherification and

amidation procedure (see synthesis section in the Supporting Information (SI)) and featured branches (two or three) of tetraethylene glycol that were terminated by −OMe, −OH, or −OSO₃⁻ groups (order of increasing hydrophilicity).[63,64] Furthermore, the Pt(II) amphiphile with a much larger hydrophobic part (branched undecyl chains) and sulfate end groups, **Pt-2xUSO₄**, was prepared by a different synthetic route (see synthesis section in the SI). The negatively charged systems were isolated as triethylammonium salts, enabling solubility in aqueous as well as organic media (see Tables S2 and S3 in the SI for details).

These Pt(II) amphiphiles differ from many other commonly used surfactants by their unusual low CAC in the micromolar range (10−50 μM) that was determined by dynamic light scattering (DLS) (see Table 1). For comparison, the CAC (or critical micelle concentration (CMC) in the context of micelles) values of sodium cholate (15 mM), SDS (8 mM), CTAB (0.9 mM), and lauryl glucoside (0.2 mM) are 2−3 orders of magnitude higher than that for the Pt(II) amphiphiles. The low CAC values are due to an interplay of supramolecular interactions such as hydrophobicity, hydrogen bonds, and Pt−Pt and $\pi-\pi$ interactions. Therefore, the assemblies are already formed in aqueous buffer at low concentrations, ensuring their role as the template in the formation of VLPs. From DLS measurements, the hydrodynamic diameter (d_{hyd}) of the resulting assemblies formed by the branched tetraethylene glycol based Pt(II) amphiphiles, such as **Pt-3xTOMe**, **Pt-3xTOH**, **Pt-3xTSO₄**, and **Pt-2xTSO₄**, were in the size range of d_{hyd} = 5−24 nm (Table 1). The markedly larger size of the noncharged micelles compared to that of analogous negatively charged micelles is in agreement with the observed behavior with different surfactants and the geometric packing model.[65] These complex aggregates can all fit inside the inner cavity of the icosahedral-shaped CCMV capsid ($d_{in} \approx$ 21 nm for T = 3 particles), as schematically depicted in Figure 1 (see Figure S17 for transmission electron microscopy (TEM) images).

Complex **Pt-2xUSO₄** possesses a hydrophobic part much larger than that of the aforementioned amphiphiles (see Scheme 1), balanced by a hydrophilic negatively charged group as the terminal unit. DLS experiments indicated the formation of very large particles ($d_{hyd} \sim$ 150 nm) upon self-assembly in aqueous buffer, featuring a low CAC of 15 μM. The TEM images (see Figure S16) show that the pure complex self-assembles in long fibers (~100−300 nm) featuring a width of around 6 nm. Similar morphologies were reported by Manners

Table 1. Physical and Photophysical Data of the Pt(II) Amphiphiles in TRIS Buffer (pH 7.2)

complex[a]	d_{hyd} (nm)[b]	CAC (mM)[c]	λ_{em} (nm)[d]	τ (ns)[e]	Φ (%)[f]
Pt-3xTOMe	24.2 ± 3.6	0.053	600	443 [367][g]	52 [36][g]
Pt-3xTOH	21.9 ± 3.3	0.024	605	552 [332][g]	60 [33][g]
Pt-3xTSO₄	5.6 ± 1.5	0.018	607	304 [139][g]	32 [7][g]
Pt-2xTSO₄	8.7 ± 2.2	0.010	612	171 [45][g]	14 [6][g]
Pt-2xUSO₄	150 ± 21[h]	0.015	578	645 [586][g]	58 [22][g,i]

[a]Measurements were performed for 0.1 mM Pt(II) amphiphile in 50 mM TRIS buffer (pH 7.2, 10 mM MgCl₂) in aerated ambient conditions. See the SI for data at different concentration of amphiphile. [b]Hydrodynamic diameter determined by DLS. [c]CAC concentration determined by DLS at fixed angle and attenuation, CAC error ~10%. Note: Appropriately dimensioned particles are necessary for the encapsulation into CCMV capsids. The CAC for the presented Pt(II) amphiphiles is here understood as the concentration at which the transition from monomers/smaller aggregates (e.g., dimers) to suitably sized aggregates (e.g., micelles) is occurring. [d]Maximum of emission determined by emission spectroscopy with excitation at 375 nm. [e]Amplitude weighted average lifetime determined by emission spectroscopy with excitation at 375 nm; τ error ~1%. [f]Emission quantum yield determined with an integrating sphere; φ error ~5%. [g]Measurements in square brackets determined at Pt complex concentrations as observed in VLP (see SI). [h]Size estimation by TEM was performed for nonspherical aggregates (see text). [i]Determination of φ by relative method.

et al. on analogues Pt(II) complexes bearing a single extended polyglycol chain ($n = 7-16$) at the ancillary ligand, and long fibers were observed only for the longest chain.[66,67]

The well-known environment- and aggregation-state-dependent emission properties of square-planar Pt(II) complexes served as a convenient, independent measure for monitoring their self-assembly in aqueous solution. As expected, both the excited-state lifetime and emission quantum yield markedly increase upon formation of aggregated structures above the CAC (Table 1). The formed assemblies possess a strong room temperature emission ($\varphi \sim 14-60\%$) featuring an extraordinary long excited-state lifetime (up to 550 ns) (see Table 1 and SI for details), in the presence of dioxygen, depending on the molecular structure of the complex. Noteworthy, contrary to common fluorophores, which suffer from aggregation-caused quenching, these platinum(II)-based phosphors render a strong luminescent material at high local and global concentrations due to their aggregation-induced emission properties. Determination of the CAC values through monitoring of the photophysical changes upon dilution of the Pt(II) amphiphiles in aqueous buffered solution yielded CAC values that well correspond to those obtained by DLS (see Table S4).[68] However, we noticed that the emission spectra, peaking around 600 nm, always resembled that of the aggregated state of Pt(II) chromophores even upon strong dilution of the formed assemblies to the nanomolar concentration regime. Usually, a weak blue-shifted emission is observed upon molecular dissolution of Pt(II) complexes due to the monomeric species unless the Pt(II) chromophores are covalently tethered together.[56] Consequently, it appears that the Pt(II) amphiphiles can form remarkably stable assemblies (containing possibly only few units) already much below their CAC, confirming the multiple intermolecular interactions.

Icosahedral VLPs Templated by TEG-Branched Pt(II) Amphiphiles. The good aqueous solubility of the Pt(II) surfactants and their low critical aggregation concentrations of $10-50~\mu M$ are important requirements for proper encapsulation experiments with CCMV coat proteins. CP isolation from CCMV was accomplished according to the literature.[24,69] In general, the preparation of VLPs was conducted as follows. First, the capsid proteins and the Pt(II) amphiphiles were mixed in a molar ratio of 1:5 in TRIS pH 7.2 buffer. The electrical neutral Pt(II) amphiphiles (**Pt-3xTOMe, Pt-3xTOH**) decorated with TEG branches cannot induce the assembly of CPs under neutral pH condition, due to the weak interactions between these amphiphiles and CPs.[70] Therefore, a passive encapsulation, in which the pH value was tuned from 7.2 to 5.1, was adopted to achieve the encapsulation (see encapsulation section in the SI for details). The assembly of VLPs is mainly driven by protein–protein interaction under weak acidic conditions. On the other hand, the negatively charged Pt(II) amphiphiles **Pt-3xTSO₄** and **Pt-2xTSO₄** underwent encapsulation at pH 7.2 with the CPs, indicating their templating effect. In this case, the assembly of VLPs was driven by the electrostatic interactions between the anionic Pt(II) amphiphiles and the positively charged CPs and by the protein–protein interactions.

Subsequently, the samples were purified and characterized by fast protein liquid chromatography (FPLC). The elution volumes around 10.8–11.3 mL for all samples indicate the formation of VLPs (Figure 2a and SI). A separation of the VLPs from remaining capsid proteins (17.5 mL) and Pt(II) assemblies was achieved for all samples. The DLS analysis
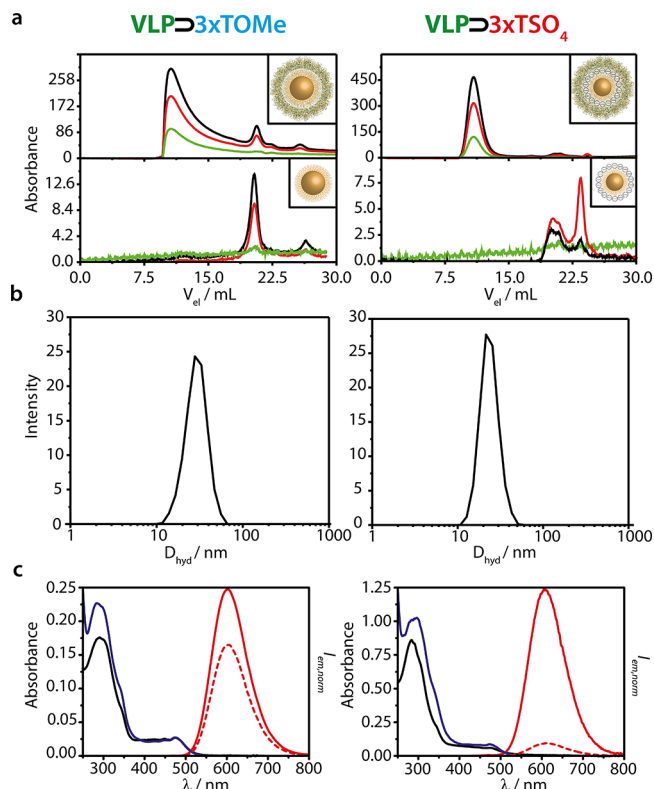

Figure 2. (a) FPLC chromatograms of **VLP⊃3xTOMe** (left) and **VLP⊃3xTSO₄** (right) and corresponding Pt amphiphile solution without capsid at 1 mM (bottom). Colors indicate absorbance wavelengths: 260 nm (red), 280 nm (black), 340 nm (green). (b) DLS intensity distributions of the **VLP⊃3xTOMe** (left) and **VLP⊃3xTSO₄** (right). (c) Absorption spectra (solid, black), excitation (solid, blue, $\lambda_{em} = \lambda_{em,max}$, arbitrary units), and emission (solid, red, $\lambda_{exc} = 405$ nm, normalized) spectra of the VLPs **VLP⊃3xTOMe** (left) and **VLP⊃3xTSO₄** (right). The quantum yield weighted emission spectra (dashed, red, $\lambda_{exc} = 405$ nm) of the corresponding Pt amphiphiles (**Pt-3xTOMe, Pt-3xTSO₄**) at the same concentration are depicted.

(Figure 2b and SI) confirms the formation of VLPs with d_{hyd} of ~28 nm for **VLP⊃3xTOMe** and **VLP⊃3xTOH** and d_{hyd} of ~18 nm for **VLP⊃3xTSO₄** and **VLP⊃2xTSO₄**. To further confirm the estimated results from FPLC and DLS, TEM experiments were performed with uranyl acetate staining. Spherical particles were observed for **VLP⊃3xTOMe** and **VLP⊃3xTOH**, with a diameter of ~28 nm; also, spherical particles for **VLP⊃3xTSO₄** and **VLP⊃2xTSO₄** but with a diameter of ~18 nm. The results are consistent with the DLS results (Figure 3a and SI).

The TEM images show that the filled particles display a spherical shape and an entirely bright contrast, whereas less filled cages appear with a dark contrast in the interior, resembling donuts. While predominantly filled VLPs were observed for the encapsulation with negative Pt(II) assemblies, the neutral analogues resulted in distributions of filled and empty VLPs. This behavior is in agreement with the different capsid formation mechanism, templated *versus* statistical by pH changes, for negatively charged and noncharged cargos, respectively. High-angle annular dark-field scanning transmission electron microscopy (HAADF-STEM, no staining) analysis reveals a high average atomic number (Z) due to the heavy Pt atoms, shown as bright spots within the dark outer low Z protein shell (Figure 3c). Accumulated energy-dispersive
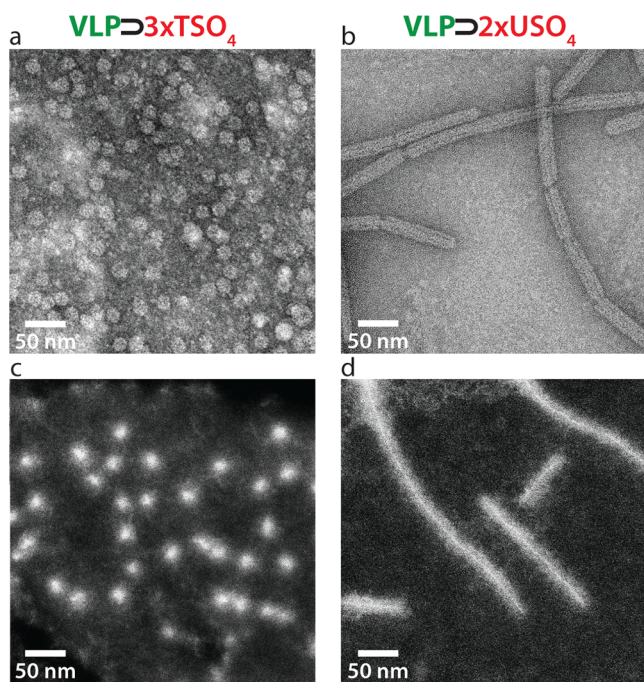
Figure 3. (a) TEM (negative stain) image of **VLP⊃3xTSO₄**. (b) TEM (negative stain) image of **VLP⊃2xUSO₄**. (c) HAADF-STEM (no staining) image of **VLP⊃3xTSO₄**. (d) HAADF-STEM (no staining) image of **VLP⊃2xUSO₄**. The scale bars are 50 nm.

X-ray spectroscopy of a set of particles also displayed characteristic platinum signals (SI).

The average loading of the Pt(II) complex per capsid was estimated from inductively coupled plasma mass spectrometry (ICP-MS) measurements. Approximately 8−20 negatively charged **Pt-3xTSO₄** and **Pt-2xTSO₄** amphiphiles were encapsulated into one virus capsid, resulting in a high local concentration of 40−100 mM (Table 2), when assuming an inner diameter of 8.5 nm for the nearly spherical icosahedral T = 1 capsid ($V \approx 321$ nm^3). The concentration enrichment by a factor of 130−310 of the Pt(II) cargo due to the templating effect is evident. The average occupation for noncharged amphiphiles was much lower (average was 1−4 per virus capsid), pointing also to a mixture of filled and empty capsids.

Table 2. Physical and Photophysical Data of the Pt(II) Amphiphiles in TRIS Buffer (pH 7.2)[a]

VLP	d_{hyd} (nm)[b]	$c_{Pt,local}$ (mM)[c]	λ_{em} (nm)[d]	τ (ns)[e]	Φ (%)[f]
VLP⊃3xTOMe	29.6 ± 1.5	0.28	601	474	51
VLP⊃3xTOH	28.7 ± 1.4	1.46	605	502[g]	54
VLP⊃3xTSO₄	18.1 ± 0.5	102.49	607	612	57
VLP⊃2xTSO₄	19.5 ± 1.6	43.19	604	620	52
VLP⊃2xUSO₄	>50 [~18][g]	5.86	600	462	23

[a]Measurements were performed with the solution isolated from FPLC (see Figure 2a). [b]Hydrodynamic diameter determined by DLS. [c]Local Pt(II) complex concentration calculated from ICP-MS (AES) data for Pt and S. [d]Maximum of emission determined by emission spectroscopy with excitation at 375 nm. [e]Amplitude weighted average lifetime determined by emission spectroscopy with excitation at 375 nm; τ error ~1%. [f]Emission quantum yield determined with an integrating sphere; φ error ~5%. [g]Size estimation by TEM was performed for nonspherical particles (see text) for the length and width (displayed in square brackets).

In particular, upon encapsulation, Pt(II) concentration enrichment for **Pt-3xTOMe** was very little and only of a factor 4 for **Pt-3xTOH** (see Table 2). The results are in agreement with a passive encapsulation mechanism. The obtained VLPs with either neutral or negative Pt(II) assemblies entrapped inside display a strong room temperature emission around 600 nm, long emission lifetimes (474−620 ns), and high quantum yields (51−57%) (see Figure 2c, Table 2, and SI), remaining unaffected by dilution or the presence of dioxygen (see photophysical analysis of VLPs in the SI for deaeration experiments). In fact, the photophysical properties of the noncharged Pt(II)-amphiphile-filled capsids resemble that of the self-assembled Pt(II) amphiphiles at high concentrations in aqueous buffer, although the bulk concentrations of Pt(II) amphiphiles are much lower than their CAC (SI, Table S1).

The observed photophysical parameters, such as a strong metal/metal-to-ligand charge transfer absorption band at 475 nm and the broad emission profiles peaking around 600 nm, are indicative of Pt−Pt interactions and thus aggregation of the Pt(II) complexes.[60,71−73] These results suggest that the Pt(II) amphiphile species are present at a high local concentration inside the filled virus capsids. The negatively charged VLPs reveal a strong enhancement of their emission quantum yield upon encapsulation into the virus capsids (factor up to 13), leveling off at the maximum values observed for the noncharged Pt(II) amphiphiles and other aqueous self-assembling Pt(II) complexes based on the same terdentate N-metallacycling ligand.[60] This increase in quantum yield of the negatively charged amphiphiles upon virus encapsulation may be due to the high local concentration inside the capsids,[23] which prevents motions of the luminophores, leading to rigid-ochromic effects.[74] The enhanced rigidity by the immobilization of the negatively charged tail in the positively charged protein shell leads most likely to a decrease in the nonradiative deactivation pathways.[75,76]

Rod-like VLPs Templated by Alkyl-Branched Pt(II) Amphiphiles. Unlike many soft artificial self-assembling systems, CCMV capsid formation is expected to show little propensity for change in shape and size, as this would potentially impact its biological function. The successful entrapment of assemblies constituted by tetraethylene glycol based Pt(II) complexes showed, however, that the morphology of the VLPs is not modified by the loaded species. Indeed, in all cases, a natively shaped icosahedral virus cage was maintained. It turns out that when the size of templates is comparable to or smaller than the inner space of the icosahedral protein cage (~21 nm), the protein−protein interaction promotes the assembly of CPs into icosahedron particles (T = 1, 2, 3) preferentially. In other words, the high shape persistence of the CCMV capsid formation overpowers the geometric preference of the amphiphile templates. We demonstrate that, through the use of a robust supramolecular template with a large size and a high aspect ratio, the template−protein interactions may force the assembly of CPs to accommodate the preferred shape of the template, resulting in VLPs with tailored nonicosahedron morphology.

To this end, the chemical structure of the Pt(II) amphiphiles was modified such that thermodynamic stable rod-like supramolecular structures were formed by the amphiphiles. Albeit overlooked by the classic packing model, the transition from spherical to extended rod-like assemblies can be triggered when the chain length or solvatophobic nature of a surfactant tail is modified.[65] We utilized this feature by exchanging the

tetraethylene glycol chains with more hydrophobic alkyl chains (undecyl), retaining the negatively charged, hydrophilic and virus−protein attracting head groups, and the Pt(II) complex core. The chemical structure of the obtained **Pt-2xUSO₄** amphiphile is shown in Scheme 1 (see the SI for synthetic procedure). Indeed, self-assembly of **Pt-2xUSO₄** in aqueous media leads to the appearance of long (>50 nm) and thin (∼6 nm) rods (see Figure S14). Their low CAC value and their characteristic photophysical properties were in accordance with a thermodynamically stable, closely packed self-aggregated structure, suggesting that these may be appropriate supramolecular templates that could induce the formation of rod-like VLPs.

As expected, mixing CPs (0.066 mM) and **Pt-2xUSO₄** amphiphiles (0.33 mM) resulted in the formation of rod-like assemblies (see encapsulation section in the SI for details). The TEM images of the resultant VLPs display predominantly cylindrical (nonicosahedral) rods (Figure 3b,d). The obtained rod-like VLPs vary in their length (100−500 nm) but possess a homogeneous thickness around 18 nm, which is comparable to the diameter of a protein icosahedron with $T = 1$ but larger than that of the self-assembled **Pt-2xUSO₄** fibers (6 nm).[77] The apparent enlarged cross section diameter suggested the formation of a protein shell around the Pt(II) complex threads. HAADF-STEM analysis displays a high average atomic number (Z) due to the heavy Pt atoms as bright lines within the dark outer low Z protein shell (Figure 3d), confirming the presence of Pt(II) inside the shell.

The obtained VLPs show room temperature emission peaking at 600 nm with a quantum yield of 23% and an excited-state lifetime of 462 ns, which are typical features for the assembled Pt(II) complexes (see photophysical analysis of VLPs in SI for details). These fibrous VLPs contained a local, concentration-enriched Pt(II) complex content similar to that of the virus capsids that were templated by negatively charged TEG-branched Pt(II) amphiphiles (Table 2).

The mechanism of the formation of rod-like VLPs is not well understood.[12] On the basis of the established quasi-equivalence model of Casper and Klug,[22] one can understand the observed spherical particles as an icosahedral organized protein shell with a triangulation of $T = 1$ (Figure 1). All negative cargos increase the local concentration of protein dimers that facilitate the formation of pentamers-of-dimers.[19] In contrast to the smaller negative assemblies (d_{hyd} < inner CCMV diameter), the larger cargo, based on **Pt-2xUSO₄** (d_{hyd} > inner CCMV diameter), perturbs the curvature for the formation of icosahedral $T = 1$ particles (Figure 1). The misalignment of pentamers avoids the closure to a spherical (icosahedral) particle, leading to elongated subunits that allow for rod-like structures via protein−protein interactions. The VLPs therefore can grow long while retaining their thickness. While our findings and explanations are in agreement with the observation and theories of other groups,[77,78] further experiments are ongoing in our laboratories to confirm the proposed mechanism.

CONCLUSION

Water-soluble Pt(II) amphiphiles decorated with tetraethylene glycol branches and sulfate groups were synthesized and probed for their self-assembly properties. The luminescent Pt(II) complexes are soluble in organic and aqueous buffered solution. In buffered solution, intense room temperature emission was observed also at low concentrations because of the self-assembly of the Pt(II) complexes. The assemblies have been

used to template CCMV proteins, yielding luminescent virus-like particles. A remarkable enhancement of the photophysical properties was observed for the negatively charged amphiphiles, rendering a VLP quantum yield of 57%. We gained a deep understanding of correlations among molecular structure, supramolecular architecture, and on the formation of VLPs. Taking advantage of the modulation of multiple interactions between templates and capsid proteins through the molecular design, it is possible to manage the self-assembly process resulting in tailored morphology of VLPs as well as functionality. The negatively charged platinum compounds induced a templated formation of VLPs, which can be icosahedral or nonicosahedral (rod-like) depending on the molecular structure of amphiphilic templates. To the best of our knowledge, this is the first example where a supramolecular material (self-assembled Pt(II) complexes) induces a shape change in the CCMV capsid formation. We envisage that different supramolecular templates can lead to a variety of shapes and stabilities of VLPs, which in turn can have a strong impact in biomedical applications.

ASSOCIATED CONTENT

Supporting Information
The Supporting Information is available free of charge on the ACS Publications website at DOI: 10.1021/jacs.7b12447.

> Experimental details, further chemical characterization and photophysical analysis, additional figures and table (PDF)

AUTHOR INFORMATION

Corresponding Authors
*j.j.l.m.cornelissen@utwente.nl
*decola@unistra.fr

ORCID
Liulin Yang: 0000-0003-3342-8137
Jeroen J. L. M. Cornelissen: 0000-0002-9728-5043
Luisa De Cola: 0000-0002-2152-6517

Author Contributions
⊥S.S. and L.Y. contributed equally.

Notes
The authors declare no competing financial interest.

REFERENCES

(1) Aida, T.; Meijer, E. W.; Stupp, S. I. *Science* **2012**, *335* (6070), 813−817.

(2) Whitesides, G. M.; Mathias, J. P.; Seto, C. T. *Science* **1991**, *254* (5036), 1312.

(3) Whitesides, G. M.; Grzybowski, B. *Science* **2002**, *295*, 2418−2421.

(4) Lehn, J. M. *Science* **2002**, *295* (5564), 2400−3.

(5) Whitesides, G. M.; Boncheva, M. *Proc. Natl. Acad. Sci. U. S. A.* **2002**, *99* (8), 4769−4774.

(6) Reinhoudt, D. N.; Crego-Calama, M. *Science* **2002**, *295*, 2403−2407.

(7) Adolph, K. W.; Butler, P. J. G. *J. Mol. Biol.* **1974**, *88* (2), 327−341.

(8) Douglas, T.; Dickson, D. P. E.; Betteridge, S.; Charnock, J.; Garner, C. D.; Mann, S. *Science* **1995**, *269*, 54−57.

(9) Douglas, T.; Young, M. *Nature* **1998**, *393* (6681), 152−155.

(10) Zlotnick, A. *J. Mol. Biol.* **1994**, *241* (1), 59−67.

(11) Liepold, L. O.; Revis, J.; Allen, M.; Oltrogge, L.; Young, M.; Douglas, T. *Phys. Biol.* **2005**, *2* (4), S166.

(12) Lavelle, L.; Gingery, M.; Phillips, M.; Gelbart, W. M.; Knobler, C. M.; Cadena-Nava, R. D.; Vega-Acosta, J. R.; Pinedo-Torres, L. A.; Ruiz-Garcia, J. *J. Phys. Chem. B* **2009**, *113* (12), 3813−3819.

(13) Putri, R. M.; Cornelissen, J. J. L. M.; Koay, M. S. T. *ChemPhysChem* **2015**, *16* (5), 911−918.

(14) Minten, I. J.; Hendriks, L. J. A.; Nolte, R. J. M.; Cornelissen, J. J. L. M. *J. Am. Chem. Soc.* **2009**, *131* (49), 17771−17773.

(15) Millán, J. G.; Brasch, M.; Anaya-Plaza, E.; de la Escosura, A.; Velders, A. H.; Reinhoudt, D. N.; Torres, T.; Koay, M. S. T.; Cornelissen, J. J. L. M. *J. Inorg. Biochem.* **2014**, *136*, 140−146.

(16) Lavelle, L.; Michel, J.-P.; Gingery, M. *J. Virol. Methods* **2007**, *146* (1−2), 311−316.

(17) Ochoa, W. F.; Chatterji, A.; Lin, T.; Johnson, J. E. *Chem. Biol.* **2006**, *13* (7), 771−778.

(18) Mukherjee, S.; Pfeifer, C. M.; Johnson, J. M.; Liu, J.; Zlotnick, A. *J. Am. Chem. Soc.* **2006**, *128* (8), 2538−2539.

(19) Tang, J.; Johnson, J. M.; Dryden, K. A.; Young, M. J.; Zlotnick, A.; Johnson, J. E. *J. Struct. Biol.* **2006**, *154* (1), 59−67.

(20) Brumfield, S.; Willits, D.; Tang, L.; Johnson, J. E.; Douglas, T.; Young, M. *J. Gen. Virol.* **2004**, *85*, 1049−1053.

(21) Goldberg, M. *Tohoku Math. J.* **1937**, *43*, 104−108.

(22) Caspar, D. L.; Klug, A. *Cold Spring Harbor Symp. Quant. Biol.* **1962**, *27*, 1−24.

(23) Brasch, M.; de la Escosura, A.; Ma, Y.; Uetrecht, C.; Heck, A. J. R.; Torres, T.; Cornelissen, J. J. L. M. *J. Am. Chem. Soc.* **2011**, *133* (18), 6878−6881.

(24) Comellas-Aragones, M.; Engelkamp, H.; Claessen, V. I.; Sommerdijk, N. A.; Rowan, A. E.; Christianen, P. C.; Maan, J. C.; Verduin, B. J.; Cornelissen, J. J.; Nolte, R. J. *Nat. Nanotechnol.* **2007**, *2* (10), 635−9.

(25) Comellas-Aragonès, M.; de la Escosura, A.; Dirks, A. J.; van der Ham, A.; Fusté-Cuñé, A.; Cornelissen, J. J. L. M.; Nolte, R. J. M. *Biomacromolecules* **2009**, *10* (11), 3141−3147.

(26) Sikkema, F. D.; Comellas-Aragones, M.; Fokkink, R. G.; Verduin, B. J. M.; Cornelissen, J. J. L. M.; Nolte, R. J. M. *Org. Biomol. Chem.* **2007**, *5* (1), 54−57.

(27) Kwak, M.; Minten, I. J.; Anaya, D.-M.; Musser, A. J.; Brasch, M.; Nolte, R. J. M.; Müllen, K.; Cornelissen, J. J. L. M.; Herrmann, A. *J. Am. Chem. Soc.* **2010**, *132* (23), 7834−7835.

(28) Chang, C. B.; Knobler, C. M.; Gelbart, W. M.; Mason, T. G. *ACS Nano* **2008**, *2* (2), 281−286.

(29) Dragnea, B.; Chen, C.; Kwak, E.-S.; Stein, B.; Kao, C. C. *J. Am. Chem. Soc.* **2003**, *125* (21), 6374−6375.

(30) Chen, C.; Daniel, M.-C.; Quinkert, Z. T.; De, M.; Stein, B.; Bowman, V. D.; Chipman, P. R.; Rotello, V. M.; Kao, C. C.; Dragnea, B. *Nano Lett.* **2006**, *6* (4), 611−615.

(31) Dixit, S. K.; Goicochea, N. L.; Daniel, M.-C.; Murali, A.; Bronstein, L.; De, M.; Stein, B.; Rotello, V. M.; Kao, C. C.; Dragnea, B. *Nano Lett.* **2006**, *6* (9), 1993−1999.

(32) Bronstein, L. M. *Small* **2011**, *7* (12), 1609−1618.

(33) Liu, A.; Traulsen, C. H. H.; Cornelissen, J. J. L. M. *ACS Catal.* **2016**, *6* (5), 3084−3091.

(34) Liu, A.; Verwegen, M.; de Ruiter, M. V.; Maassen, S. J.; Traulsen, C. H. H.; Cornelissen, J. J. L. M. *J. Phys. Chem. B* **2016**, *120* (26), 6352−6357.

(35) de la Escosura, A.; Janssen, P. G. A.; Schenning, A. P. H. J.; Nolte, R. J. M.; Cornelissen, J. J. L. M. *Angew. Chem., Int. Ed.* **2010**, *49* (31), 5335−5338.

(36) Ng, B. C.; Chan, S. T.; Lin, J.; Tolbert, S. H. *ACS Nano* **2011**, *5* (10), 7730−7738.

(37) Liu, Z.; Qiao, J.; Niu, Z.; Wang, Q. *Chem. Soc. Rev.* **2012**, *41* (18), 6178−6194.

(38) Wen, A. M.; Steinmetz, N. F. *Chem. Soc. Rev.* **2016**, *45* (15), 4074−4126.

(39) Yang, L.; Liu, A.; Cao, S.; Putri, R. M.; Jonkheijm, P.; Cornelissen, J. J. L. M. *Chem. - Eur. J.* **2016**, *22* (44), 15570−15582.

(40) Steed, J. W.; Atwood, J. L. *Supramolecular Chemistry*; Wiley-VCH: Weinheim, Germany, 2009.

(41) Bibal, B.; Mongin, C.; Bassani, D. M. *Chem. Soc. Rev.* **2014**, *43* (12), 4179−4198.

(42) Ayme, J.-F.; Beves, J. E.; Leigh, D. A.; McBurney, R. T.; Rissanen, K.; Schultz, D. *Nat. Chem.* **2012**, *4* (1), 15−20.

(43) Wörsdörfer, B.; Woycechowsky, K. J.; Hilvert, D. *Science* **2011**, *331* (6017), 589.

(44) Yu, C.; Mosbach, K. *J. Org. Chem.* **1997**, *62* (12), 4057−4064.

(45) Prins, L. J.; Reinhoudt, D. N.; Timmerman, P. *Angew. Chem., Int. Ed.* **2001**, *40* (13), 2382−2426.

(46) Sasaki, E.; Böhringer, D.; van de Waterbeemd, M.; Leibundgut, M.; Zschoche, R.; Heck, A. J. R.; Ban, N.; Hilvert, D. *Nat. Commun.* **2017**, *8*, 14663.

(47) Biedermann, F.; Schneider, H.-J. *Chem. Rev.* **2016**, *116* (9), 5216−5300.

(48) Chandler, D. *Nature* **2005**, *437* (7059), 640−7.

(49) Li, I. T. S.; Walker, G. C. *Acc. Chem. Res.* **2012**, *45* (11), 2011−2021.

(50) Schneider, H.-J. *Acc. Chem. Res.* **2015**, *48* (7), 1815−1822.

(51) Wagner, J. P.; Schreiner, P. R. *Angew. Chem., Int. Ed.* **2015**, *54* (42), 12274−12296.

(52) Fuguet, E.; Ràfols, C.; Rosés, M.; Bosch, E. *Anal. Chim. Acta* **2005**, *548* (1−2), 95−100.

(53) Techen, A.; Hille, C.; Dosche, C.; Kumke, M. U. *J. Colloid Interface Sci.* **2012**, *377* (1), 251−261.

(54) Marsh, D. *Handbook of Lipid Bilayers*; CRC Press: Boca Raton, FL, 2013.

(55) Avanti Polar Lipids Inc.: Critical Micelle Concentrations (CMCs); https://avantilipids.com/tech-support/physical-properties/cmcs/ (accessed March 20, 2017).

(56) Sinn, S.; Biedermann, F.; Vishe, M.; Aliprandi, A.; Besnard, C.; Lacour, J.; De Cola, L. *ChemPhysChem* **2016**, *17* (12), 1829−34.

(57) El Garah, M.; Sinn, S.; Dianat, A.; Santana-Bonilla, A.; Gutierrez, R.; De Cola, L.; Cuniberti, G.; Ciesielski, A.; Samori, P. *Chem. Commun. (Cambridge, U. K.)* **2016**, *52* (74), 11163−6.

(58) Aliprandi, A.; Mauro, M.; De Cola, L. *Nat. Chem.* **2016**, *8* (1), 10−5.

(59) Liptrot, D. J.; Power, P. P. *Nature Reviews Chemistry* **2017**, *1*, 0004.

(60) Sinn, S.; Biedermann, F.; De Cola, L. *Chem. - Eur. J.* **2017**, *23* (8), 1965−1971.

(61) Allampally, N. K.; Bredol, M.; Strassert, C. A.; De Cola, L. *Chem. - Eur. J.* **2014**, *20* (51), 16863−16868.

(62) Mauro, M.; Aliprandi, A.; Cebrian, C.; Wang, D.; Kubel, C.; De Cola, L. *Chem. Commun.* **2014**, *50* (55), 7269−7272.

(63) Müller, M. K.; Brunsveld, L. *Angew. Chem., Int. Ed.* **2009**, *48* (16), 2921−2924.

(64) Kim, B. R.; Lee, H.-G.; Kang, S.-B.; Sung, G. H.; Kim, J.-J.; Park, J. K.; Lee, S.-G.; Yoon, Y.-J. *Synthesis* **2012**, *44* (01), 42−50.

(65) Nagarajan, R. *Langmuir* **2002**, *18* (1), 31−38.

(66) Robinson, M. E.; Nazemi, A.; Lunn, D. J.; Hayward, D. W.; Boott, C. E.; Hsiao, M.-S.; Harniman, R. L.; Davis, S. A.; Whittell, G. R.; Richardson, R. M.; De Cola, L.; Manners, I. *ACS Nano* **2017**, *11* (9), 9162−9175.

(67) Robinson, M. E.; Lunn, D. J.; Nazemi, A.; Whittell, G. R.; De Cola, L.; Manners, I. *Chem. Commun.* **2015**, *51* (88), 15921−15924.

(68) Biedermann, F. Self-Assembly in Aqueous Media. *Comprehensive Supramolecular Chemistry II*; Elsevier: Oxford, 2017; pp 241−268.

(69) Verduin, B. J. M. *FEBS Lett.* **1974**, *45* (1), 50−54.

(70) Sun, J.; DuFort, C.; Daniel, M.-C.; Murali, A.; Chen, C.; Gopinath, K.; Stein, B.; De, M.; Rotello, V. M.; Holzenburg, A.; Kao, C. C.; Dragnea, B. *Proc. Natl. Acad. Sci. U. S. A.* **2007**, *104* (4), 1354−1359.

(71) Septiadi, D.; Aliprandi, A.; Mauro, M.; De Cola, L. *RSC Adv.* **2014**, *4* (49), 25709−25718.

(72) Miskowski, V. M.; Houlding, V. H. *Inorg. Chem.* **1989**, *28* (8), 1529−1533.

(73) Ma, B.; Li, J.; Djurovich, P. I.; Yousufuddin, M.; Bau, R.; Thompson, M. E. *J. Am. Chem. Soc.* **2005**, *127* (1), 28−29.

(74) Genovese, D.; Aliprandi, A.; Prasetyanto, E. A.; Mauro, M.; Hirtz, M.; Fuchs, H.; Fujita, Y.; Uji-I, H.; Lebedkin, S.; Kappes, M.; De Cola, L. *Adv. Funct. Mater.* **2016**, *26* (29), 5271−5278.

(75) Kubicki, J.; Maciejewski, A.; Milewski, M.; Wrozowa, T.; Steer, R. P. *Phys. Chem. Chem. Phys.* **2002**, *4* (2), 173−179.

(76) Dsouza, R. N.; Pischel, U.; Nau, W. M. *Chem. Rev.* **2011**, *111* (12), 7941−7980.

(77) Prasad, B. V.; Schmid, M. F. *Advances in experimental medicine and biology* **2012**, *726*, 17−47.

(78) Bancroft, J. B.; Hills, G. J.; Markham, R. *Virology* **1967**, *31* (2), 354−379.